Lab on a Chip

Cite this: *Lab Chip*, 2012, **12**, 4724–4731

www.rsc.org/loc

PAPER

Single neuron capture and axonal development in three-dimensional microscale hydrogels†

Yantao Fan,‡[a] Feng Xu,‡*[bc] Guoyou Huang,[c] Tian Jian Lu[c] and Wanli Xing*[ad]

Received 2nd April 2012, Accepted 8th June 2012
DOI: 10.1039/c2lc40312a

Autapse is an unusual type of synapse generated by a neuron on itself. The ability to monitor axonal growth of single neurons and autapse formation in three-dimensions (3D) may provide fundamental information relating to many cellular processes, such as axonal development, synaptic plasticity and neural signal transmission. However, monitoring such growth is technically challenging due to the requirement for precise capture and long-term analysis of single neurons in 3D. Herein, we present a simple two-step photolithography method to efficiently capture single cells in microscale gelatin methacrylate hydrogel rings. We applied this method to capture and culture single neurons. The results demonstrated that neural axons grew and consequently formed axonal circles, indicating that our method could be an enabling tool to analyze axonal development and autapse formation. This method holds great potential for impact in multiple areas, such as neuroscience, cancer biology, and stem cell biology.

Introduction

Single cell analysis provides crucial information on many cellular processes, such as embryonic development,[1] tumor heterogeneity,[2] and neuronal polarity.[3] However, most existing studies are based on a population of cells that only reflect average cellular behavior. With advances in micro- and nano-techniques, many methods (*e.g.*, microfluidics,[4] surface modification,[5] bioprinting,[6] dielectrophoresis[7] and optical tweezers[8]) have been developed to unravel various cellular processes, such as cell differentiation,[9] tumor progression[10] and cell-cell/environment interaction,[11] at the single cell level. However, these methods are currently based on two-dimensional (2D) monolayer cell cultures, which may not accurately reflect natural processes. Cells exist in a three-dimensional (3D) environment *in vivo* and accumulating evidence indicates that 3D cell cultures better mimic native environments and processes compared to 2D[12]. Therefore, it is of great importance to develop an effective method for single cell capture and analysis in a 3D microenvironment.

In vitro 3D single cell analysis is urgently needed in neuroscience. It is well known that neural axons project over long distances to their target neurons to form synapses *in vivo*. Scientifically, proper axonal development determines how neural circuits function (*e.g.*, synaptic plasticity) at the tissue level, as well as human perception (*e.g.*, sensing, learning, and memory) at the organ level. Clinically, axonal damage is involved in many nerve traumas (*e.g.*, spinal cord injuries) and neurodegenerative diseases (*e.g.*, Alzheimer's disease). The ability to track single axonal development and synaptogenesis is essential for an improved understanding of these scientific and clinical problems. It was originally considered that a neural synapse could only form between neurons. However, a single neuron's axon can autonomously project back upon its own soma, forming an "autapse" (also called "self-synapse" or "recurrent synapse").[13] Autapses commonly exist in various brain regions, including the neocortex,[14] hippocampus,[15] cerebellum,[16] substantia nigra[17] and striatum.[18] Autapses can be used as simplified model systems to study various neural behaviors, such as synaptic electrophysiology, neural vesicle trafficking, and synaptic plasticity. Therefore, numerous *in vitro* model systems have been developed, most of which are based on single neurons cultured on a substrate patterned with isolated "micro-islands".[19] Using these autapse model systems,[20] many molecule-function experiments (*e.g.*, synaptotagmin 1 function[15]) have been performed. However, there are several challenges associated with such model systems. Particularly, these models are 2D with limited spatial control of axonal growth and autapse formation. Therefore, there is an urgent need for a suitable 3D model with precise control for single-neuron capture, axon navigation, and autapse formation in a 3D microenvironment mimicking nature.

[a]*Medical Systems Biology Research Center, School of Medicine, Tsinghua University, Beijing, China 100086*
[b]*The Key Laboratory of Biomedical Information Engineering of Ministry of Education, Xi'an Jiaotong University School of Life Science and Technology, Xi'an, China 710049. E-mail: fengxu@mail.xjtu.edu.cn*
[c]*Biomedical Engineering and Biomechanics Center, Xi'an Jiaotong University, Xi'an, China 710049*
[d]*National Engineering Research Center for Beijing Biochip Technology, 18 Life Science Parkway, Beijing, 102206, China. E-mail: wlxing@mail.tsinghua.edu.cn*
† Electronic supplementary information (ESI) available: See DOI: 10.1039/c2lc40312a
‡ Authors contributed equally to this work

Herein, we report a two-step photolithography method to efficiently capture a single cell in a 3D gelatin methacrylate (GelMA) hydrogel ring. Gelatin, a component of the GelMA hydrogel, is derived from denatured collagen, which is abundant in the native extracellular matrix (ECM), including neural ECM.[21] Therefore, GelMA contains the natural cell binding motifs, such as Arg-Gly-Asp (RGD), which elicit improved cell-hydrogel interactions and provide cells with a 3D microarchitecture that mimics ECM *in vivo*.[22] Particularly, GelMA is photo-polymerizable, thus precise spatial control can be achieved to fabricate intricate microarchitectures. These favorable properties of GelMA, combined with a two-step photolithography method, provide a simple platform for single cell analysis in a 3D microenvironment. We applied this method to capture single neurons in GelMA rings, which grew into axonal circles (defined as the axon projecting along the GelMA ring back to its own soma) in a 3D microloop. The method developed here is controllable, rapid, and cost-effective, holding great potential for applications in multiple areas, such as drug screening (*e.g.*, tumor progression) and axonal biology (*e.g.*, autapse function).

Materials and methods

Synthesis of GelMA

GelMA hydrogel is a photo-polymerizable methacrylated gelatin with good biocompatibility.[22] Gelatin can be engineered to become photo-crosslinkable *via* the controlled incorporation of methacrylate groups to the amine-containing side groups, which enables the fabrication of complex geometries. Additionally, GelMA is an attractive candidate for rapid *in situ* photopolymerization. In this study, we synthesized GelMA following a previously reported protocol.[23] Gelatin (type A, 300 bloom from porcine skin), methacrylic anhydride (MA), and 3-(trimethoxysilyl)propyl methacrylate (TMSPMA) were purchased from Sigma-Aldrich (St. Louis, MO). The photoinitiator 2-hydroxy-1-[4-(hydroxyethoxy)phenyl]-2-methyl-1-propanone (Irgacure 2959) was purchased from CIBA Chemicals (Basel, Switzerland). The synthesized GelMA was suspended in Dulbecco's phosphate buffered saline (DPBS, 5%, w/v) and mixed with 0.5% (w/v) Irgacure 2959.

Preparation of cell-laden GelMA hydrogel suspension

NIH 3T3 fibroblasts from the cell bank of the Chinese Academy of Sciences and rat cortical neurons were used for the single cell capture efficiency studies and axonal development analysis, respectively. To track the cells, 3T3 cells were trypsinized and labeled with CellTracker (CellTracker™ Red CMTPX) according to the manufacturer's instructions. Then, labeled 3T3 cells were suspended in GelMA precursor solution containing 0.5% (w/v) Irgacure 2959 at four different concentrations, *i.e.*, 0.2, 0.7, 1.5, and 10.0 $\times$ 10^6 cells ml^{-1}.

Dissociated cortical cell cultures were prepared following a protocol in the literature.[24] All animal work was approved by the Medicine Animal Care and Use Committee of Xi'an Jiaotong University, and abided by national guidelines for animal welfare. Briefly, cortical tissue was taken from postnatal 1 day old (PD 1) Sprague Dawley® rats (from the Fourth Military Medical University, Xi'an, China) and dissociated by trituration after digestion with papain (20 U ml^{-1}). The cells were then suspended in a medium consisting of 50% minimal essential medium (MEM) supplemented with 10% fetal bovine serum and 50% NB medium (Neurobasal™ with B27 supplement and 0.5 mM glutamine). The medium that was initially added to the cultures was also supplemented with 25 μM glutamate and 25 μM β-mercaptoethanol. Dissected neurons were suspended in 5% (w/v) GelMA precursor solution at a concentration of 0.7 $\times$ 10^6 cells ml^{-1}.

Two-step photolithography for single cell capture in GelMA

Controlled photo-polymerization of GelMA and cell capture was achieved by using a simple two-step photolithography technique, Fig. 1. We designed two types of masks, mask I and mask II (ESI, Fig. S1†), which were custom-tailored from Newway Electronic Co. (Shenzhen, CHN). The gapped loops in mask I were 20 μm wide, 400 μm in diameter, and 100 μm in the gap dimension (Fig. 1e); a 6 $\times$ 6 loop matrix was patterned with the same loops. We designed loops 400 μm in diameter (approximately 1250 μm long perimeter) according to the neural axon's projection capacity, which permits axons to extend over and distinguish axons from dendrites.[25] Capture dots with a diameter of 150 μm in mask II were designed to spatially match loops in mask I. To better illustrate the two-step photolithography process, we added two kinds of fluorescent dyes respectively to the GelMA precursor solution for the two steps of photolithography. Specifically, Fluorescein isothiocyanate-dextran FITC (Sigma-Aldrich) at a concentration of 10 μg ml^{-1} was added to the GelMA precursor solution for the lithography step to form gapped GelMA loops. Rhodamine B (Sigma-Aldrich) at the same concentration was added to the GelMA precursor solution for the second-step lithography to form GelMA capture dots. These two chemicals are commonly used for hydrogel staining. After the two-step lithography, a GelMA hydrogel ring was formed with a loop (FITC-dextran in green) and capture dot (Rhodamine B in red), Fig. 1f. Images of each hydrogel ring were taken using an inverted fluorescence microscope (Olympus IX81) equipped with a filter cube. The 3D GelMA hydrogel rings were fabricated on a TMSPMA-treated glass coverslip, which was used to avoid cell adherence on the coverslip due to its hydrophobic nature.[26] The thickness of the GelMA hydrogel ring could be adjusted by the height of the spacer (using the coverslip). In this work, we fabricated GelMA hydrogel rings with a thickness of 150 μm to provide enough growth space in the vertical direction, in view of the appropriate 15–30 μm diameter of a pyramidal neuron or the 0.2–1 μm diameter of an axon. With all these designs, the resulting GelMA rings had dimensions of 400 (loop diameter) $\times$ 150 (capture dot diameter) $\times$ 150 μm (GelMA ring height), as shown in Fig. 1e and the ESI (Fig. S1†).

For the first photo-polymerization step, 20 μl of cell-free GelMA precursor solution was dropped onto a TMSPMA-treated glass coverslip and cross-linked using mask I and UV light for 40 s at a power density of 2.95 mW cm^{-2} (Omnicure® S2000), resulting in gapped GelMA loops (Fig. 1b). The glass coverslips containing these GelMA loops were washed with DPBS. Then another 20 μl of 3T3 cells suspended in GelMA precursor solution was dropped onto the former coverslip

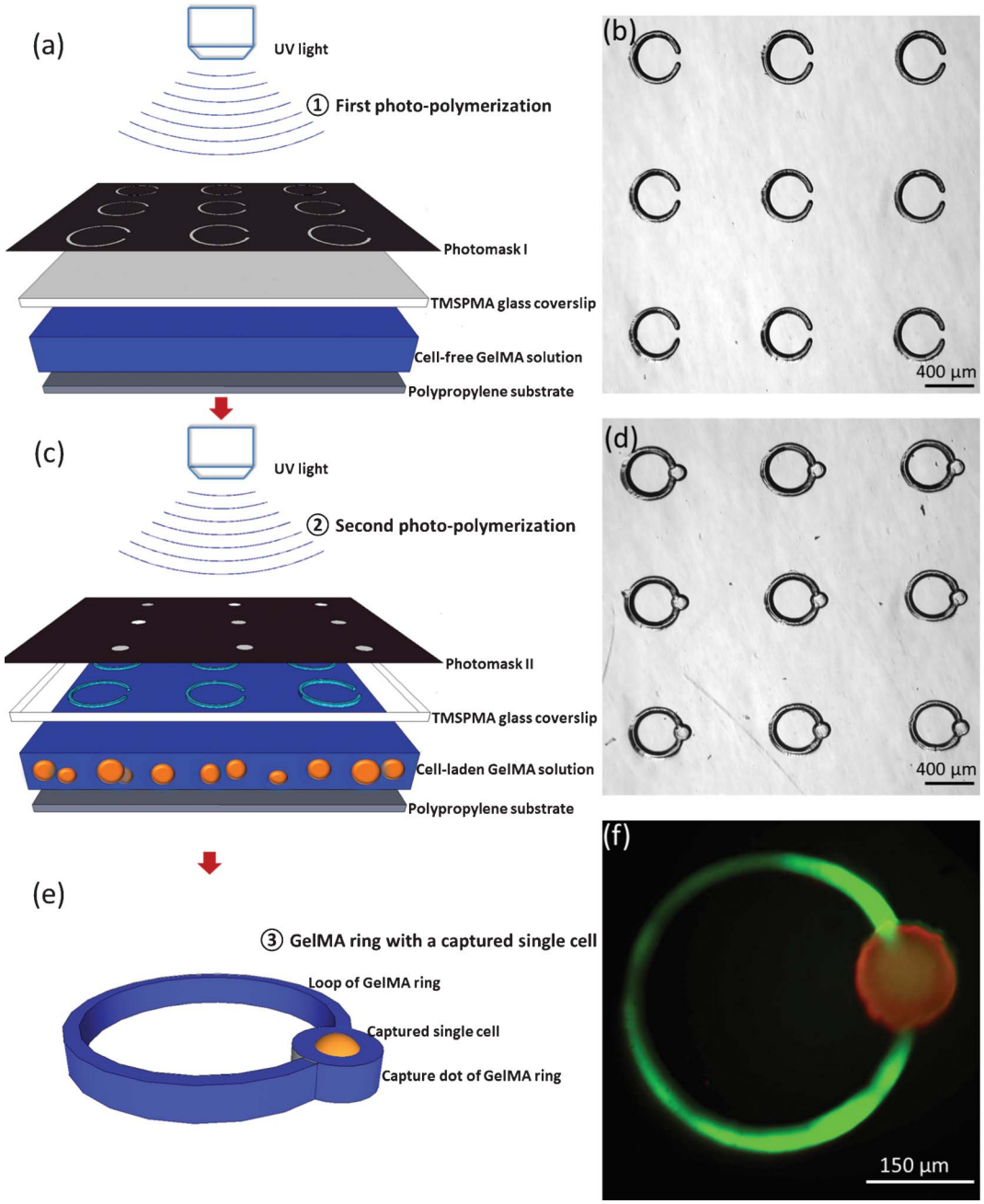

Fig. 1 Two-step photolithography for 3D capture of single cells in GelMA hydrogel. Schematic illustrations (a, c and e) of the two-step process of GelMA hydrogel photo-polymerization. GelMA precursor solution was pipetted between two glass slides separated by a 150 μm spacer and exposed to 2.95 mW cm^{-2} UV light (40 s) through mask I. A corresponding GelMA layer was patterned on a TMSPMA glass slide to form a gapped 3D hydrogel loops to define a cell growth trace. A second cell-suspended GelMA precursor solution was then dropped on top of the formed gapped loops, shown in (b). The 150 μm capture dots were defined on the gap position using 2.95 mW cm^{-2} UV light (20 s) through mask II, and an arrayed hydrogel ring matrix was achieved, as shown in (d). The aligned loop and dot formed an intact ring with a single cell trapped in the desired position (e), providing a 3D matrix for directed cell adhesion, spreading and growth after trapping. (f) Fluorescence images of a GelMA hydrogel ring with loop (FITC-dextran in green) and capture dot (Rhodamine B in red), respectively.

containing the GelMA loops, covered with mask II and exposed to 2.95 mW cm^{-2} UV light for 20 s. The non-crosslinked cell suspension was washed away using DPBS, resulting in a GelMA ring with cells captured only in the capture dots (Fig. 1e, f). Here, we define a hydrogel ring as a "single cell ring" if only a single cell was captured in this ring, as a "no cell ring" if no cell was captured, or as a "multi-cell ring" if more than one cell was captured in a hydrogel ring, respectively. Single cell capturing efficiency was defined as the percentage of the single cell rings from the total number of GelMA hydrogel rings after photolithography. No cell capturing efficiency and multi-cell capturing efficiency were defined similarly. Cell and hydrogel ring imaging was performed using an inverted fluorescence microscopy (Olympus IX81). The number of 3T3 cells in each hydrogel ring was counted using NIH software ImageJ. The tests were repeated 3-6 times for statistical analysis.

Culture and staining of single 3T3 cells

Captured single 3T3 cells in GelMA hydrogel rings were cultured in DMEM supplemented with 10% FBS in a 5% CO_2 atmosphere at 37 °C for 2–3 weeks. The medium was changed every 2 days. To better understand the states of the 3T3 cells in the 3D GelMA hydrogel ring, we stained the cell bodies and nuclei of these 3T3 cells with 2 μg ml^{-1} calcein-AM green (Invitrogen) in DPBS and 1 μg ml^{-1} DAPI (Invitrogen) in DPBS, respectively. Calcein-AM is cleaved by esterases in live cells to yield cytoplasmic green fluorescence, and DAPI binds to nucleic acids to yield blue fluorescence. GelMA hydrogel rings with 3T3 cells were incubated with the staining solution for 20 min and visualized with phase-contrast and fluorescence imaging.

Capture and culture of single neurons

Dissected neurons were suspended in 5% (w/v) GelMA precursor solution at 0.7 × 10^6 cells ml^{-1}. Single neuron capture was performed following the similar procedure for 3T3 cell capture. For the neuron culture, glass slides with neuron-captured GelMA hydrogel rings were placed in a six-well plate filled with 3 ml neural culture medium. These neurons were maintained in a culture at 37 °C with an atmosphere of 95% air and 5% CO_2. The medium was changed twice a week by replacing half the culture medium. The eural axons and nuclei of the cells were stained with calcein-AM green (Invitrogen) and DAPI (Invitrogen), respectively. The degree and behavior of axonal growth or neural migration were directly observed using phase-contrast and fluorescence imaging. This protocol was performed in 4 weeks.

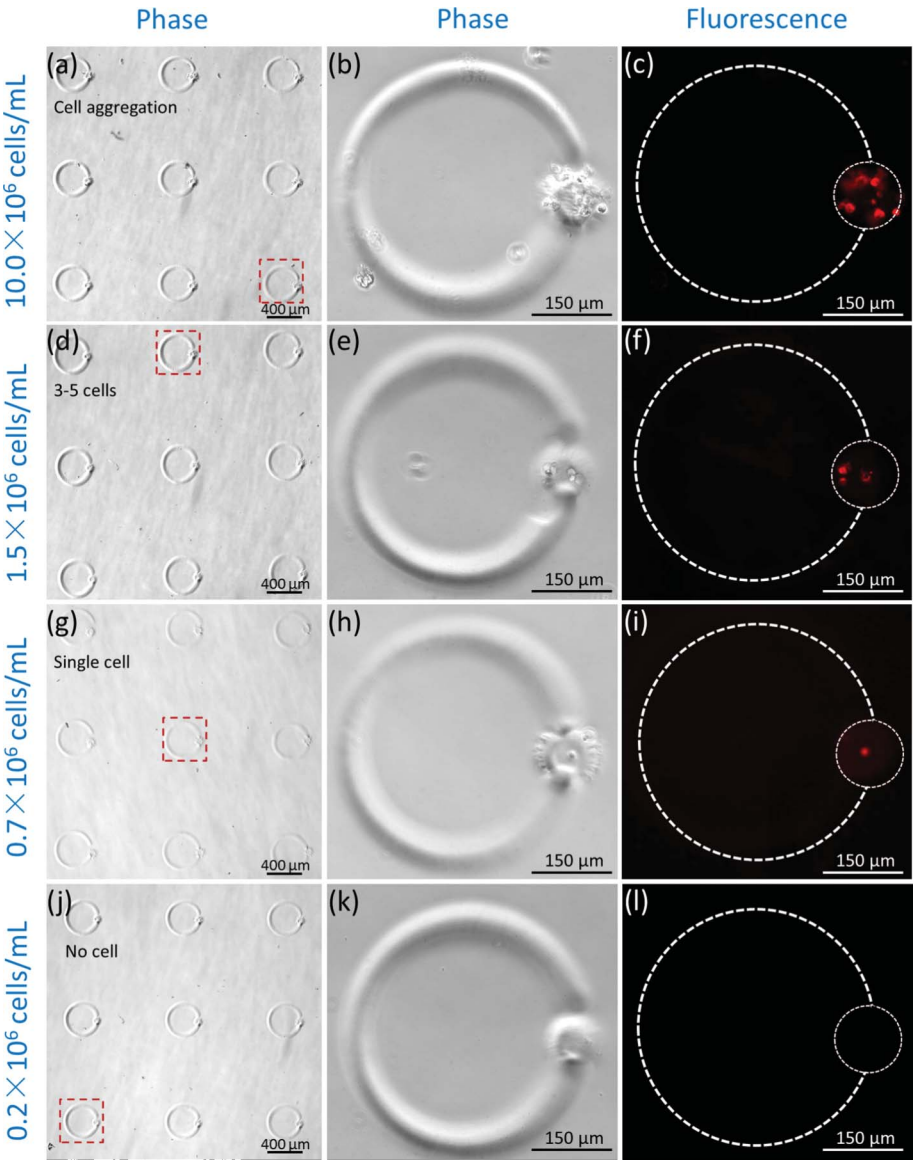

Fig. 2 Single cell capture in GelMA hydrogel. Phase-contrast (magnified) and fluorescence images of 3T3 cells (CellTracker red) in GelMA at different cell concentrations: (a–c) 10 × 10^6 cells ml^{-1}, (d–f) 1.5 × 10^6 cells ml^{-1}, (g–i) 0.7 × 10^6 cells ml^{-1}, and (j–l) 0.2 × 10^6 cells ml^{-1}. Dotted lines indicate the boundary of the ring. (j–l) Typical images of the proliferation of captured cells from single cell level to a cell population in the hydrogel ring after 2 weeks of culture. The dashed areas in (a), (d), (g), and (j) were enlarged in (b), (e), (h), and (k), respectively.

Poisson distribution statistics

Poissonian curves of single cell capturing probability were plotted using MATLAB (MathWorks Inc.). The k value was set at 1 for three curves. The λ value was set at 0.2060, 0.8242 and 1.8545 for curves of 50, 100, and 150 μm, respectively.

Statistical analysis

Data were compared using one-way analysis of variance (ANOVA) followed by Tukey's post-hoc comparisons for repeated measures. A statistical significance threshold was set at 0.05 for all tests (with $p < 0.05$). Error bars in the figures represent mean ± standard deviation.

Results and discussion

In our system, the single cell capturing efficiency depends on cell concentration and GelMA ring design. Theoretically, when dropping cell-laden GelMA precursor solution onto a coverslip (Fig. 1c), the distribution of cells is random in each location of GelMA hydrogel capture dots. The volume of the capture dot is fixed and independent of the number of captured cells, with the number of captured cells per capture dot following a Poisson distribution after photolithography.[27] The λ value (*i.e.*, the expected value of the cell capture event) here was determined by cell concentration and the volume of hydrogel capture dot. For the Poisson distribution, we simulated the influence of cell concentration and GelMA ring design on the single cell capturing efficiency (ESI, Fig. S2†). Considering that a pyramidal neuron's diameter is appropriately 30 μm, we simulated three capture dot diameters, *i.e.*, 50, 100, and 150 μm. As shown in the ESI (Fig. S1†), the Poissonian curve reaches its maxima when the x value is between 0.375 and 0.85, indicating that an optimal cell concentration for high single cell capturing efficiency should be between 0.375–0.85 × 10^6 cells ml^{-1} with respect to the capture dot diameter from 100–150 μm. To facilitate the alignment operation between the two-step lithography, we ultimately chose 150 μm as our GelMA ring design.

To experimentally evaluate the dependency of single cell capturing efficiency on cell concentration, we captured 3T3 cells in the GelMA hydrogel at different concentrations. Considering that variables in experiments (*e.g.*, variations in hydrogel size or cell concentration) will result in deviations in efficiency not dictated by Poisson statistics, we tested a large range of cell concentrations, *i.e.*, four concentrations of 0.2, 0.7, 1.5, 10.0 × 10^6 cells ml^{-1} while keeping GelMA capture dot size at a constant diameter of 150 μm (Fig. 2). We observed that cells were captured at all concentrations, as shown in both phase contrast and fluorescence images (Fig. 2a–i). At the highest cell concentration (10.0 × 10^6 cells ml^{-1}), each capture dot was filled with cells that tended to aggregate due to the high concentration and limited space (Fig. 2a–c). We also quantified the efficiency of single cell capture for concentrations of 1.5 × 10^6, 0.7 × 10^6, and 0.2 × 10^6 cells ml^{-1} are 36.9 ± 1.5, 46.4 ± 7.8, and 29.8 ± 2.9% (Fig. 3a). For a cell concentration of 1.5 × 10^6 cells ml^{-1}, 3–5 cells on average (55.2 ± 5.40% of "multi-cells" percentage) were captured in each hydrogel ring. For a cell concentration of 0.7 × 10^6 cells ml^{-1}, we observed that many of the rings contained single cells: 46.4 ± 7.8% GelMA rings were loaded with "single cell", whereas rings with "no cell" and "multi-cells" represented 24.0 ± 7.6% and 29.6 ± 7.4% of the total, respectively. When the cell concentration decreased further, the cell capture efficiency significantly decreased ($p < 0.05$, $n = 4$), and there were almost no captured cells in most of the hydrogel rings (Fig. 2j–l). We found that the single cell capture efficiency was only 29.8 ± 2.9% for a cell concentration of 0.2 × 10^6 cells ml^{-1}. Also, the single cell capture efficiency between the concentrations of 0.7 × 10^6 and 1.5 × 10^6 cells ml^{-1} (46.4 ± 7.8 and 36.9 ± 1.5%, respectively) is significantly different

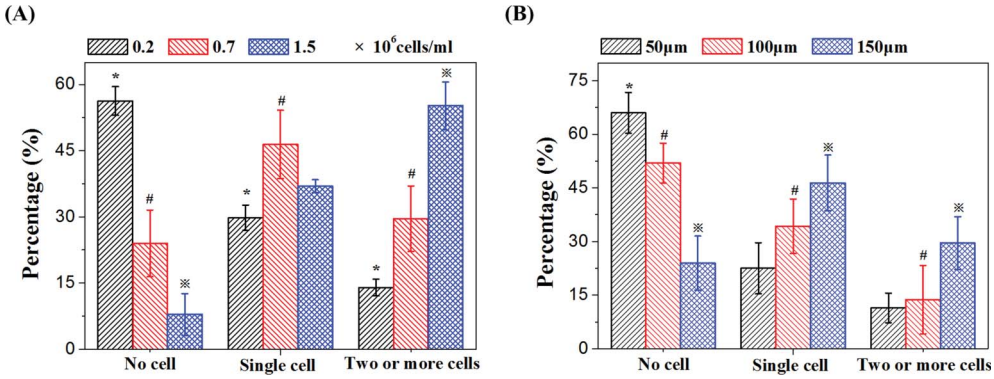

Fig. 3 Influence of cell concentration on cell capture efficiency. (a) Summary of the calculated average cell capture rate at the corresponding cell concentrations. The percentage of "no cell", "single cell", or "two or more cells" was quantified using images by counting the number of CellTracker-labeled 3T3 cells within the hydrogel rings; "*" indicates the comparison between 0.2 × 10^6 and 0.7 × 10^6 cells ml^{-1}; "#" indicates the comparison between 0.7 × 10^6 and 1.5 × 10^6 cells ml^{-1}; and "※" indicates the comparison between 0.2 × 10^6 and 1.5 × 10^6 cells ml^{-1}. Independent experimental repetitions were performed for the data analysis, *e.g.*, $n = 4$ for the 0.2 × 10^6 cells ml^{-1} concentration, $n = 6$ for the 0.7 × 10^6 cells ml^{-1} concentration, and $n = 5$ for the 1.5 × 10^6 cells ml^{-1} concentration. (b) Quantitative plot demonstrating high single cell capturing efficiency when cell concentration was about 0.7 × 10^6 cells ml^{-1}. A number of images were taken to extract quantitative information of capture efficiency after cell capture. The number of captured cells gradually increased with increasing capture dot diameter; "*" indicates the comparison between 50 and 100 μm; "#" indicates the comparison between 100 and 150 μm; and "※" indicates the comparison between 50 and 150 μm. Independent experimental repetitions were performed for the data analysis, *e.g.*, $n = 3$ for the 50 μm capture dot diameter, $n = 5$ for the 100 μm capture dot diameter, and $n = 6$ for the 150 μm capture dot diameter.

($p < 0.05$, $n = 6$). Thus, the concentration of 0.7×10^6 cells ml^{-1} was adopted for further experiments. This result is in accordance with the previous Poissonian simulation, *i.e.*, 0.7×10^6 cells ml^{-1} is within the predicted optimal concentration of 0.375–0.85 $\times 10^6$ cells ml^{-1}.

To experimentally validate if 150 μm was the optimal diameter for a high single cell capturing efficiency, we assessed the cell capture dot sizes (diameters of 50, 100, and 150 μm, respectively) under a cell concentration of 0.7×10^6 cells ml^{-1}. We observed that the single cell capture efficiency increased significantly ($p < 0.05$, n=3–6) with increasing capture dot size, *i.e.*, 22.5 $\pm$ 7.2, 34.3 $\pm$ 7.6, and 46.4 $\pm$ 7.8% for a dot size of 50, 100, and 150 μm, respectively (Fig. 3b). Hereafter, we used a cell concentration of 0.7×10^6 cells ml^{-1} and a dot diameter of 150 μm to achieve a relatively high single cell capture efficiency.

To establish a 3D single cell analysis platform, we first tested our method on 3T3 cells. We captured and cultured single 3T3 cells for 2 weeks, and monitored their growth over time. Typically, the captured 3T3 cells started spreading after 10 h (Fig. 4a, b). The 3D structure of the GelMA hydrogel is characterized as being porous and interconnected. The captured single 3T3 cell in the GelMA ring was provided with sufficient nutrients. Compared to a 2D culture, a single 3T3 cell can spread in 3D *via* integrin-mediated cell adhesion to bind to motifs (such as RGD) in the GelMA scaffold. Resembling native ECM, GelMA hydrogel also promotes cell migration and proliferation. The long-term culture of the captured single 3T3 cells confirmed this. These cells then migrated and proliferated along and within the GelMA hydrogel rings (Fig. 4c, d and ESI, Fig. S3†), and finally formed a loop of monoclonal cell populations (Fig. 4e–h). It is known that tumor cell genomes quickly become twisted in unusual ways as the tumor cells evolve. Thus, these results suggest a feasible method to study the cellular behavior of cancer cells (such as cancer heterogeneity) in a physiologically relevant state. For example, by capturing and culturing individual cancer cells, this method could allow: (i) investigation of tumorigenesis at the individual cell scale, (ii) detailed development of tumor evolution and metastasis, and (iii) structural control as well as external factors' influence on tumors.

To investigate axonal development at the single cell level, we captured and cultured single neurons using our method. We also tracked axonal growth by taking images daily. These time-lapse observations show a single neuron's neurite initiation, axonal growth, and finally axonal circle formation process from day 1 to week 3 (Fig. 5). The initiation of neurite growth occurred at a time of approximately 1 day (Fig. 5a–c), and then the axon projected along the GelMA loop during the following days of culture (Fig. 5d–f). The first encounter of the growth cone with its own cell body occurred at approximately week 3 after extending through the entire GelMA loop. Fig. 5g–i shows an *in vitro* 3D axonal circle of a single neuron cultured in a GelMA hydrogel ring. Calcein-AM staining revealed the neural soma and its axon at the same time, while DAPI staining demonstrated that only a single neuron was captured in this GelMA ring (Fig. 5h). The bright dot indicated by the arrow in Fig. 5h is an axonal intumescentia, not another neuron. Further typical axonal growth images at different culture time points are shown in the ESI, Fig. S4†.

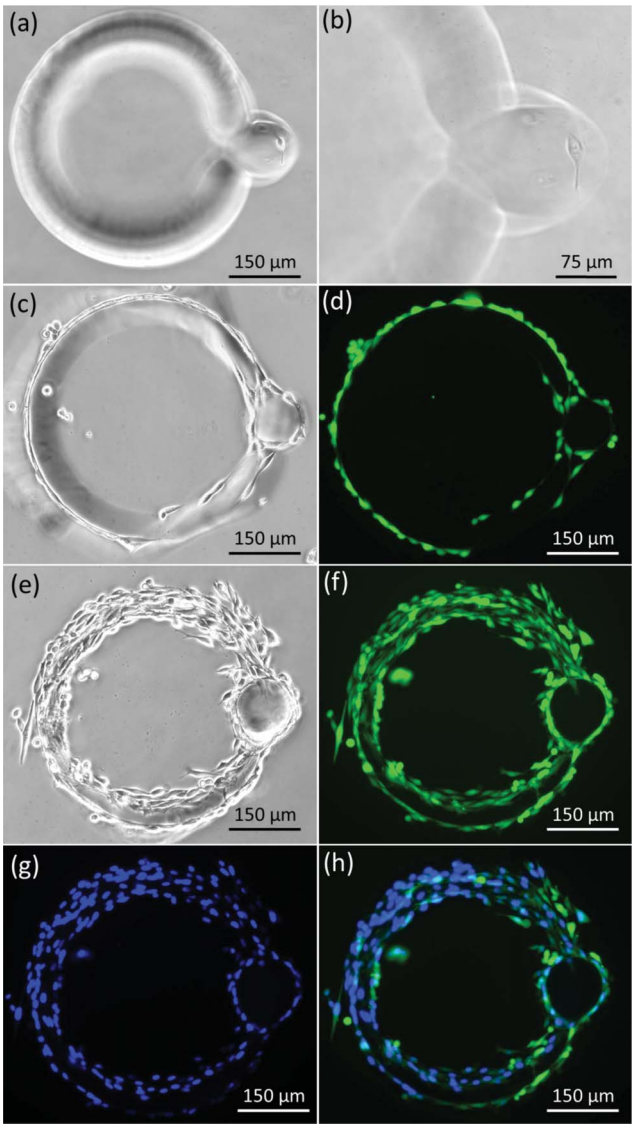

Fig. 4 Time-lapse images of a captured single 3T3 cell demonstrate its proliferation in the 3D GelMA ring. (a, b) The proliferation of the captured single cell after 10 h culture; (c–f) images of the cell proliferation and a monoclonal 3T3 population during 2 weeks of culture; (d, f) calcein-AM staining fluorescence images (live cells are shown in green); (g) DAPI staining image (nuclei are shown in blue); (h) merged image of (d, f, and g). It should be noted that the monoclonal 3T3 population in the GelMA ring was evolved from one initial single cell. (These images are from different samples because the cells can no longer be cultured after staining.)

For the GelMA hydrogel rings with a thickness of 150 μm, the captured single neuron's neurite initiation and axonal development occurred in 3D. *In vivo*, neural axons can project over long distances to find the target neuron, a process that is mediated by complex interactions with signal factors and the ECM environment.[28] Two major mechanisms involved in this phenomenon have been identified, *i.e.*, contact attraction/repulsion and chemoattraction/chemorepulsion.[29] In this work, the ECM-mimicking 3D structure of the GelMA hydrogel acted as a scaffold to support these neural processes, mainly *via* the contact attraction mechanism. In addition, all behaviors of the captured

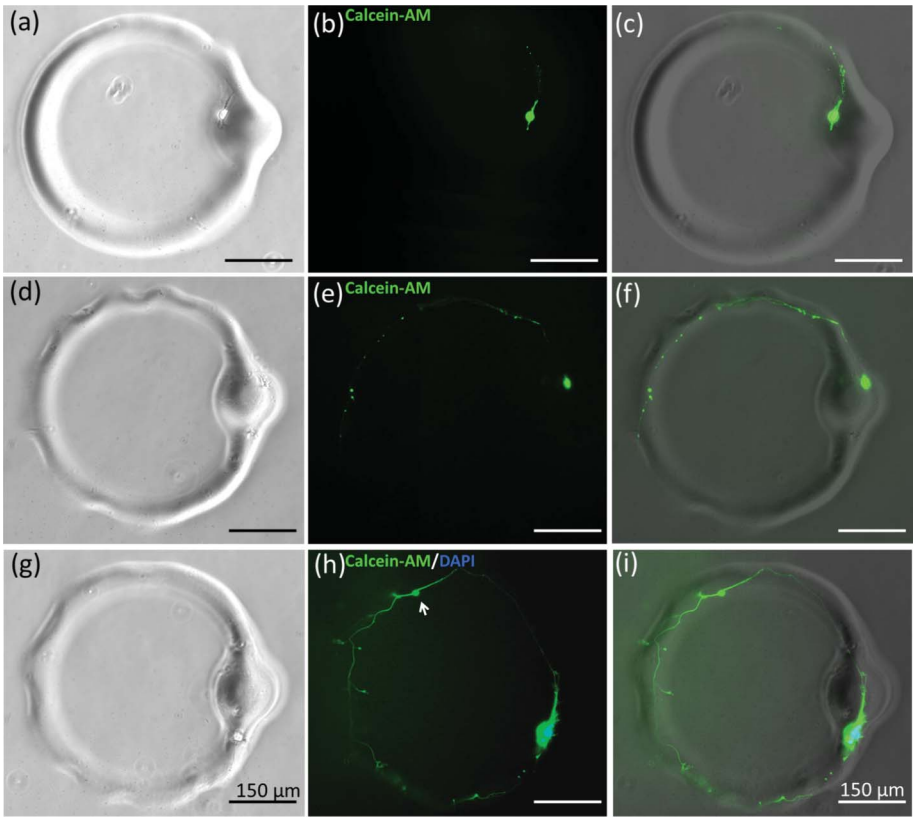

Fig. 5 Phase-contrast images of a captured single neuron's axonal projection in the GelMA hydrogel ring (a, d, g), fluorescence image (b, e, h), and the corresponding merged images (c, f, i) show the result of calcein-AM staining of the captured single neuron in the GelMA hydrogel ring, where axons can be clearly observed. The entire period from initial growth (day 1) until the final formation of the axonal circle was approximately 3 weeks. (a–c) Show the initiation of neurite cultured in hydrogel microstructure, 24 h after photo-polymerization (Day 1). A captured single neuron in the GelMA hydrogel ring started spreading out axon. (d–f) The axon grew along the GelMA ring. (g–i) An axonal circle formed after 3 weeks of culture. The loop composed of neural soma and axon was clearly observed in bright green (calcein-AM), suggesting good viability. (h, i) Nucleus in blue stained with DAPI and the merged image. The bright dot indicated by the arrow in (h) is an axonal intumescentia, not another neuron, which is also confirmed by DAPI staining. Scale bar = 150 μm. (These images are from different samples because the cells can no longer be cultured after staining.)

single neuron, such as cellular spreading, neurite initiation and axonal development, were confined to the GelMA hydrogel ring since there was no polylysine modification of the coverslip substrate, which is mandatory for a 2D neural culture in a Petri dish. Thus, the soma of the captured single neuron was confined to the GelMA capture dot (ESI, Fig. S1c† and Fig. 5d–f) while its axon gradually projected along the GelMA hydrogel loop (ESI, Fig. S1b† and Fig. 5d–f) with prolonged culture time. The platform therefore allows the isolation of axons from neural soma as well as the investigation of axon development at the single neuron level.

The ability to precisely probe, monitor and manipulate the axonal growth of a single neuron independent of its soma will enable us to study axonal biology at the single cell level and in a 3D microenvironment. Moreover, investigation of synapse formation and maintenance in single neuron cultures will enable the elucidation of mechanisms of synaptic plasticity and neural signal transmission. Autapse cultures, as a single-neuron experimental model, have indicated signal fast spiking,[30] retrograde signaling,[31] and synaptic transmission[32] as well as analysis of neuromolecule-function.[15] For example, autapses have been viewed as a simplified model of short-term analogue memory storage.[33] However, these autapses' functions *in vivo* remain uncertain. It is difficult for the existing 2D autapse model (*i.e.*, microisland culture) to spatially control autapse formation (ESI, Fig. S5†) and to distinguish autapses among numerous neurites (*e.g.*, axons, axon collaterals, and dendrites). Compared to the existing 2D models, our 3D method has the advantage of precise spatial control for autapse formation. Therefore, our method, together with high-resolution imaging, patch clamping, and other powerful techniques, will enable one to study autapses in a 3D native mimicking microenvironment. To our knowledge, this is the first attempt to build autapses in a controllable 3D microstructure.

Conclusions

In summary, we have developed a simple two-step lithography method to capture single cells in a 3D photo-polymerizable GelMA ring. Single cell capture with precise spatial control and high efficiency was achieved by adjusting the GelMA ring gap size and cell concentration. We applied this method to capture and culture single neurons, and found that neural axons grew in 3D and formed axonal circles.

The developed platform can be used to track autapse formation and autaptic transmission at the single cell level in 3D to uncover fundamental neuroscience mechanisms, especially

regarding *in vivo* autapse function. Specifically, the 3D geometry and assembly of the GelMA hydrogel can be conveniently and programmably engineered with micrometer-scale resolution by tailoring photomasks using computer-aided-design software and this multi-step lithography method. This advantage results in precise control of the axonal growth route of captured individual neurons by designing the geometry of the GelMA hydrogel loop. Autapses from conventional "microisland" cultures are randomly formed onto the neurons own dendrites or somata. However, the location of autapse formation in our method can be controlled. In addition, the cultures can be maintained for prolonged periods (2–3 weeks), allowing further experiments and measurements. It has been reported that 80% of pyramidal cells in the neocortex form autapses.[34] Currently, little is known about the functions of this large percentage of autapses *in vivo*. We have noticed that autapses, in terms of their unusual cellular interactions, contribute to unusual neural circuits that are also characterized by many clinical mental disorders (*e.g.*, autism, schizophrenia, and tristimania).[35] This implies that there may exist a specific correlation between autapses and mental disorders (especially autism). Exploring autapse function is therefore particularly important to reveal information for new therapies. A significant potential work might consist of electrophysiological recording, related gene identification and drug screening on the native-like autapses formed by the captured single neurons in 3D GelMA hydrogel rings.

Notably, there are no chemoattractants or growth factors used in this study. Recently, advances in hydrogel chemistry and cell biology have enabled the incorporation of molecules such as chemoattractants or growth factors into hydrogels to modulate cellular behaviors.[36] GelMA hydrogel possesses a large percentage of functional groups (*e.g.*, carboxylic, amino, and hydroxyl groups), which allows GelMA to be covalently modified or non-covalently mixed with growth factors. Therefore, one potential work to be developed is to investigate designable chemoattraction/chemorepulsion of single axonal growth by modifying the 3D GelMA hydrogel with nerve growth factor (NGF). The trapping pattern of our method can also be easily modified by designing different photomasks to capture multiple amounts and types of cells in designed capture dots of a GelMA ring. This will enable researchers to study temporally controlled cell–cell interactions, such as cancer cell–healthy cell interactions to mimic tumor invasion.

Acknowledgements

This research was funded by the National 863 Project of the Chinese Ministry of Education (2012AA020101). GH, TJL, and FX were partially supported by the National Natural Science Foundation of China (10825210, 31050110125) and the National 111 Project of China (B06024).

References

1 M. Kerszberg and L. Wolpert, *Cell*, 2007, **130**, 205–209.
2 P. Dalerba, T. Kalisky, D. Sahoo, P. S. Rajendran, M. E. Rothenberg, A. A. Leyrat, S. Sim, J. Okamoto, D. M. Johnston, D. Qian, M. Zabala, J. Bueno, N. F. Neff, J. Wang, A. A. Shelton, B. Visser, S. Hisamori, Y. Shimono, M. van de Wetering, H. Clevers, M. F. Clarke and S. R. Quake, *Nat. Biotechnol.*, 2011, **29**, 1120–1127.
3 N. Arimura and K. Kaibuchi, *Nat. Rev. Neurosci.*, 2007, **8**, 194–205.
4 J. Gao, X. F. Yin and Z. L. Fang, *Lab Chip*, 2004, **4**, 47–52.
5 O. Palyvoda, A. N. Bordenyuk, A. K. Yatawara, E. McCullen, C. C. Chen, A. V. Benderskii and G. W. Auner, *Langmuir*, 2008, **24**, 4097–4106.
6 F. Xu, S. J. Moon, A. E. Emre, E. S. Turali, Y. S. Song, S. A. Hacking, J. Nagatomi and U. Demirci, *Biofabrication*, 2010, **2**, 014105.
7 D. Jiang, C. E. Sims and N. L. Allbritton, *Electrophoresis*, 2010, **31**, 2558–2565.
8 K. Schutze and G. Lahr, *Nat. Biotechnol.*, 1998, **16**, 737–742.
9 C. B. Franco, C. C. Chen, M. Drukker, I. L. Weissman and S. J. Galli, *Cell Stem Cell*, 2010, **6**, 361–368.
10 N. Navin, J. Kendall, J. Troge, P. Andrews, L. Rodgers, J. McIndoo, K. Cook, A. Stepansky, D. Levy, D. Esposito, L. Muthuswamy, A. Krasnitz, W. R. McCombie, J. Hicks and M. Wigler, *Nature*, 2011, **472**, 90–94.
11 E. E. Hui and S. N. Bhatia, *Proc. Natl. Acad. Sci. U. S. A.*, 2007, **104**, 5722–5726.
12 D. W. Hutmacher, *Nat. Mater.*, 2010, **9**, 90–93.
13 H. van der Loos and E. M. Glaser, *Brain Res.*, 1972, **48**, 355–360.
14 P. Somogyi, G. Tamas, R. Lujan and E. H. Buhl, *Brain Res. Rev.*, 1998, **26**, 113–135.
15 T. Nishiki and G. J. Augustine, *J. Neurosci.*, 2004, **24**, 6127–6132.
16 C. Lu, Z. Fu, I. Karavanov, R. P. Yasuda, B. B. Wolfe, A. Buonanno and S. Vicini, *J. Neurophysiol.*, 2006, **96**, 2282–2294.
17 A. B. Karabelas and D. P. Purpura, *Brain Res.*, 1980, **200**, 467–473.
18 R. J. Preston, G. A. Bishop and S. T. Kitai, *Brain Res.*, 1980, **183**, 253–263.
19 T. G. Allen, *Nat. Protoc.*, 2006, **1**, 2543–2550.
20 J. M. Bekkers, *Curr. Biol.*, 2009, **19**, R296–298.
21 J. S. Cheng, D. B. Dubal, D. H. Kim, J. Legleiter, I. H. Cheng, G. Q. Yu, I. Tesseur, T. Wyss-Coray, P. Bonaldo and L. Mucke, *Nat. Neurosci.*, 2009, **12**, 119–121.
22 A. I. van den Bulcke, B. Bogdanov, N. De Rooze, E. H. Schacht, M. Cornelissen and H. Berghmans, *Biomacromolecules*, 2000, **1**, 31–38.
23 J. W. Nichol, S. T. Koshy, H. Bae, C. M. Hwang, S. Yamanlar and A. Khademhosseini, *Biomaterials*, 2010, **31**, 5536–5544.
24 G. Xiang, L. Pan, L. Huang, Z. Yu, X. Song, J. Cheng, W. Xing and Y. Zhou, *Biosens. Bioelectron.*, 2007, **22**, 2478–2484.
25 A. M. Taylor, M. Blurton-Jones, S. W. Rhee, D. H. Cribbs, C. W. Cotman and N. L. Jeon, *Nat. Methods*, 2005, **2**, 599–605.
26 Z. Cao, B. Du, T. Chen, J. Nie, J. Xu and Z. Fan, *Langmuir*, 2008, **24**, 12771–12778.
27 A. C. Rowat, J. C. Bird, J. J. Agresti, O. J. Rando and D. A. Weitz, *Proc. Natl. Acad. Sci. U. S. A.*, 2009, **106**, 18149–18154.
28 M. Tessier-Lavigne and C. S. Goodman, *Science*, 1996, **274**, 1123–1133.
29 M. A. Wolman, Y. Liu, H. Tawarayama, W. Shoji and M. C. Halloran, *J. Neurosci.*, 2004, **24**, 8428–8435.
30 A. Bacci, J. R. Huguenard and D. A. Prince, *J. Neurosci.*, 2003, **23**, 859–866.
31 M. E. Sheffield, T. K. Best, B. D. Mensh, W. L. Kath and N. Spruston, *Nat. Neurosci.*, 2011, **14**, 200–207.
32 R. Saada, N. Miller, I. Hurwitz and A. J. Susswein, *Curr. Biol.*, 2009, **19**, 479–484.
33 H. S. Seung, D. D. Lee, B. Y. Reis and D. W. Tank, *J. Comput. Neurosci.*, 2000, **9**, 171–185.
34 J. Lubke, H. Markram, M. Frotscher and B. Sakmann, *J. Neurosci.*, 1996, **16**, 3209–3218.
35 H. Akil, S. Brenner, E. Kandel, K. S. Kendler, M. C. King, E. Scolnick, J. D. Watson and H. Y. Zoghbi, *Science*, 2010, **327**, 1580–1581.
36 R. G. Wylie, S. Ahsan, Y. Aizawa, K. L. Maxwell, C. M. Morshead and M. S. Shoichet, *Nat. Mater.*, 2011, **10**, 799–806.